

Xu, Q., Gong, P., Chen, T., Michael, J. & Li, S. (2015). Modelling and characterization of NAND flash memory channels. *Measurement*, 70, pp. 225-231. doi: 10.1016/j.measurement.2015.04.003



**CITY UNIVERSITY
LONDON**

[City Research Online](#)

Original citation: Xu, Q., Gong, P., Chen, T., Michael, J. & Li, S. (2015). Modelling and characterization of NAND flash memory channels. *Measurement*, 70, pp. 225-231. doi: 10.1016/j.measurement.2015.04.003

Permanent City Research Online URL: <http://openaccess.city.ac.uk/14144/>

Copyright & reuse

City University London has developed City Research Online so that its users may access the research outputs of City University London's staff. Copyright © and Moral Rights for this paper are retained by the individual author(s) and/ or other copyright holders. All material in City Research Online is checked for eligibility for copyright before being made available in the live archive. URLs from City Research Online may be freely distributed and linked to from other web pages.

Versions of research

The version in City Research Online may differ from the final published version. Users are advised to check the Permanent City Research Online URL above for the status of the paper.

Enquiries

If you have any enquiries about any aspect of City Research Online, or if you wish to make contact with the author(s) of this paper, please email the team at publications@city.ac.uk.

Modelling and Characterization of NAND Flash Memory Channels

Quan Xu^a, Pu Gong^a, Thomas M. Chen^{a,*}, John Michael^b, Shancang Li^c

^a*School of Mathematics, Computer Science and Engineering, City University London,
Northampton Square, London EC1V 0HB, UK*

^b*iStorage Limited, 13 Alperton Lane, Perivale, Middlesex UB6 8DH, UK*

^c*Institute for Informatics and Digital Innovation, Edinburgh Napier University, Edinburgh,
EH10 5DT, UK*

Abstract

The threshold voltage distribution after ideal programming in NAND flash memory cells is usually distorted by a combination of the random telegraph noise (RTN), cell-to-cell Interference (CCI), and the retention process. To decide the original bits more accurately in this scenario, a precise channel model shall be utilized on the basis of the measured threshold voltages. This paper aims to characterize these various distortions occurring in multi-level cell (MLC) flash memories. A mathematical description of the overall distribution for the total flash channel distortion is presented. The final threshold voltage distribution for each symbol of MLC flash is also characterized, which is important for calculating the exact soft decisions of cell bits and the application of advanced flash error correction. The results of the theoretical analysis have been validated through Monte Carlo simulations of the flash channel.

Keywords: NAND flash, error correction codes, flash channel, soft decisions

1. Introduction

NAND flash memory is becoming essential as the storage media to a range of applications today, such as flash drive, solid state disks, mobile phone, etc.

*Corresponding author

Email addresses: Quan.Xu.1@city.ac.uk (Quan Xu), Pu.Gong.1@city.ac.uk (Pu Gong), Tom.Chen.1@city.ac.uk (Thomas M. Chen), john@istorage-uk.com (John Michael), S.Li@napier.ac.uk (Shancang Li)

Generally speaking, the original information is firstly encoded with an error
5 correction code, and the resulted bit sequence is stored to flash memories by
programming the cell threshold voltages to different levels. Measurement over
the flash memory channel is then used for the decoding and decision-making of
the original bits.

As program-erase (P/E) cycles and the data retention time increase, the
10 threshold voltage distribution of sub-20 nm NAND flash memory is commonly
distorted severely, making the measured channel outputs extremely unreliable.
On the other hand, advanced soft decision-based error correction codes (ECC)
such as low density parity check codes (LDPC) [1, 2, 3] are gradually replacing
traditional ECC using hard decisions in the current flash memory design practice
15 in order to compensate for the high raw bit error probability. Decoding of these
soft decision-based algorithms depends heavily on the accuracy of the reliability
information obtained by multiple memory measurements, or a channel model
with exactly characterized threshold voltage distribution.

Generally, Gaussian-based channel models are widely used in the study of
20 flash coding. For instance, pulse amplitude modulation (PAM) with Gaussian
noise of same variances is used by Wang et al. to model flash cell threshold volt-
age levels [4]. Sun et al. approximated the flash channel with a similar model
except with different variances for each level [5]. A similar model was used by
Zhou et al. to explore the advantages of dynamic thresholds in flash reading
25 [6]. All of these Gaussian-based channel models are relatively simple allowing
researchers to focus more on the coding aspects. However, the fact that the real
distribution is far different from the approximate model degrades the correctness
of reliability information. Therefore, other researchers have sought to character-
ize the final voltage distribution more accurately based on these noise sources.
30 Lee and Sung developed parameter estimation algorithms to find the means and
variances of the threshold voltage, which is more exact because the parameters
are estimated separately for each symbol. However, the final distributions are
still approximated as Gaussian mixtures [7]. Dong et al. treated the cell-to-cell
interference as the dominant distortion and mathematically derived the final

35 voltage distribution, but the results were approximate due to the neglect of the other noises [8]. Another idea is to observe the channel from the statistical view and ignore the probability forms of distortions. The channel model based on this idea has been proposed recently by Moon et al. and successfully used to instruct the error correction coding [9, 10]. However, such statistical way is not
40 capable to provide clear mathematical descriptions of the channel noises and final threshold voltage distribution.

This paper derives exact probability density functions for the combined channel noises and the final cell threshold voltage that used in calculating the soft channel information. The approach here uses the characteristic function of each
45 noise distribution to determine the cumulative influence caused by all noises. For the case of 4-level MLC flash memory, the noise distribution is calculated and compared to simulation results. The final distributions of each symbol are determined in explicit formulas providing a way to calculate the soft information. Simulation results over the channel with specified P/E cycling number
50 and retention time demonstrate the theoretical deductions are consistent with the practical channel outputs.

This paper is organized as follows. Section 2 explains the basic operations and noise sources of NAND flash memory. In Section 3, the various noises are explained, and characteristic functions are used to investigate the channel
55 distribution. The final distributions for each symbol in 4-level MLC are given as a case study. Simulation results are also presented in this section.

2. Noises in NAND Flash Memory

The information stored in NAND flash memory is physically expressed in the cell threshold voltages that are programmed by injecting a certain amount
60 of electrical charge into the memory cells. An erase operation involves removing the charges before programming a memory cell, which sets its threshold voltage to the lowest voltage window. Due to operation variability, the threshold voltage distribution of erased cells tends to have a wide Gaussian-like distribution, which

can be approximately modelled as

$$p_e(x) = \frac{1}{\sigma_e \sqrt{2\pi}} e^{-(x-\mu_e)^2/2\sigma_e^2} \quad (1)$$

65 where μ_e and σ_e are the mean and standard deviation of the erased state.

For programming, a scheme called incremental stair pulse programming (ISPP) is used to achieve a tight threshold voltage bound for the representation of each symbol (or level) of the MLC. Let V_p denote the verify voltage of the target programmed level, and ΔV_{pp} the program step voltage. Ideally, the
70 ISPP results in an uniform distribution over $[V_p, V_p + \Delta V_{pp}]$ which has width of ΔV_{pp} . Suppose V_p and $V_p + \Delta V_{pp}$ for the k -th programmed level are denoted as $V_l^{(k)}$ and $V_r^{(k)}$, respectively. The threshold voltage distribution of the k th programmed level after ideal programming can be modelled as

$$p_p^{(k)}(x) = \begin{cases} \frac{1}{\Delta V_{pp}}, & V_l^{(k)} \leq x \leq V_r^{(k)} \\ 0, & \text{else} \end{cases} \quad (2)$$

Thus, the initial cell threshold voltages of K -level MLC flash memory, de-
75 noted as $V_i^{(k)}$ ($0 \leq k \leq K - 1$) have the following distributions

$$V_i^{(k)} \sim p_i^{(k)}(x) = \begin{cases} p_e(x), & k = 0 \\ p_p^{(k)}(x), & 1 \leq k \leq K - 1 \end{cases} \quad (3)$$

Nevertheless, the above ideal distribution can be significantly distorted in practice by three types of noises: RTN, CCI, and charge loss in retention. These noises are shown in the MLC flash channel model in Fig. 1. In the model, $V_f^{(k)}$ ($0 \leq k \leq K - 1$) is the final cell threshold voltage, and ΔV_{RTN} , ΔV_{CCI}
80 and ΔV_{ret} are the threshold voltage shifts caused by RTN, CCI and retention noise, respectively.

RTN is caused by the electrons capture and emission developed over P/E cycling, and it directly results in the threshold voltage shift and fluctuation. The probability density function of ΔV_{RTN} can be modeled as a symmetric

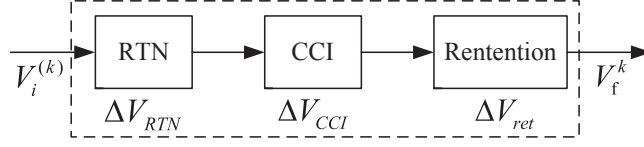


Figure 1: Noise and Interferences of the MLC flash memory

85 exponential function

$$\Delta V_{RTN} \sim p_r(x) = \frac{1}{2\lambda_r} e^{-|x|/\lambda_r} \quad (4)$$

where the parameter λ_r scales with the P/E cycling number N in an approximate power-law fashion, i.e., λ_r is approximately proportional to N^α .

Due to the parasitic capacitor-coupling effect, the threshold voltage shift of one cell affects the neighboring cells, resulting in CCI. The threshold voltage
 90 shift of a victim cell caused by CCI, denoted ΔV_{CCI} , can be estimated as

$$\Delta V_{CCI} = \sum_l \delta V^{(l)} \gamma^{(l)} \quad (5)$$

where $\delta V^{(l)}$ represents the threshold voltage shift of one interfering cell which is programmed after the victim cell, and γ^l is the coupling ratio subject to the parasitic capacitance between the interfering cell and the victim cell.

In the NAND all-bit-line structure, a victim cell is affected by three surrounding cells that are programmed after it, one along the vertical direction
 95 with γ_y while two along the two diagonal directions with γ_{xy} . Here we ignore the CCI from the two diagonal directions and treat γ_y as a constant to simplify the mathematical derivations in Section 3.

In addition to RTN and CCI, the cell threshold voltage may be reduced by
 100 interface trap recovery and electron detrapping. This is referred to as the data retention limitation. It has been demonstrated that ΔV_{ret} can be approximately modelled as a Gaussian distribution $\mathcal{N}(\mu_d, \sigma_d^2)$, where both μ_d and σ_d^2 scale to N in an approximate power-law fashion, and scale to the retention time t in a logarithmic fashion. Besides, the significance of μ_d and σ_d^2 is also proportional

105 to the initial threshold voltage $V_i^{(k)}$.

3. Characterization of Flash Memory Channel

As mentioned earlier, the goal of this work is to characterize the flash channel exactly in terms of the probability density functions of noises and cell threshold voltages. A mathematical formulation for the overall distributions of the noises
 110 shown in the channel model presented in Section 2 will be derived. Then the final threshold voltage distribution of each level of the memory will be found.

3.1. Distributions of Flash Channel Noises

Let ΔV denote the threshold voltage shift induced by noises, and $\tilde{p}(x)$ the probability density function of ΔV . In the channel model shown in Fig. 1, ΔV
 115 is the sum of the three shifts:

$$\begin{aligned}\Delta V &= \Delta V_{RTN} + \Delta V_{CCI} - \Delta V_{ret} \\ &= \Delta V_{RTN} + \gamma_y \cdot \delta V - \Delta V_{ret}\end{aligned}\tag{6}$$

Let $\Delta V_{(n)}$ represent the threshold voltage shift when the interfering cell in the vertical direction is being programmed to the n th state, and let $\tilde{p}_{(n)}(x)$ represent the probability density function of $\Delta V_{(n)}$. We have

$$\Delta V_{(n)} = \Delta V_{RTN} + \gamma_y(V_{(n)} - V_{(0)}) - \Delta V_{ret}\tag{7}$$

Assuming that the interfering cells have the same probability to be programmed to each symbol, the overall distribution of total noises induced threshold voltage shifts can be approximated as
 120

$$\Delta V \sim \tilde{p}(x) = \frac{1}{K} \sum_{n=0}^{K-1} \tilde{p}_{(n)}(x)\tag{8}$$

Next, we first derive $\tilde{p}_{(n)}(x)$ and use it to find $\tilde{p}(x)$ for the overall distribution according to (8). Considering all K possible levels for n , (7) can be rewritten

as

$$\Delta V_{(n)} = \begin{cases} \Delta V_{RTN} - \Delta V_{ret}, & n = 0 \\ \Delta V_{RTN} + \gamma_y V_i^{(n)} - \gamma_y V_i^{(0)} - \Delta V_{ret}, & 1 \leq n \leq K - 1 \end{cases} \quad (9)$$

125 In order to obtain $\tilde{p}_{(n)}(x)$, we need to calculate the convolution of probability density functions of all components in the equation above, but multiple convolutions is computationally difficult. As a simpler alternative, we use characteristic functions instead of convolutions. The characteristic functions of the major components in (9) are the following:

$$\Delta V_{RTN} \rightarrow c_{RTN}(\xi) = \frac{1}{1 + \lambda_r^2 \xi^2} \quad (10)$$

$$-\Delta V_{ret} \rightarrow c_{ret}(\xi) = e^{-\frac{1}{2} \sigma_d^2 \xi^2} \cdot e^{-i \xi \mu_d} \quad (11)$$

$$-\gamma_y V_i^{(0)} \rightarrow c_e(\xi) = e^{-\frac{1}{2} \sigma_e^2 \gamma_y^2 \xi^2} \cdot e^{-i \xi \mu_e \gamma_y} \quad (12)$$

$$\gamma_y V_i^{(n)} \rightarrow c_n(\xi) = \frac{1}{i \xi \gamma_y \Delta V_{pp}} \left(e^{i \xi \gamma_y V_r^{(n)}} - e^{i \xi \gamma_y V_l^{(n)}} \right), \quad (13)$$

$$1 \leq n \leq K - 1$$

130 For $1 \leq n \leq K - 1$, we split the right side of (9) into two parts: $\Delta V_{(n)} = V_1 + V_2$ with $V_1 = \Delta V_{RTN} + \gamma_y V_i^{(n)}$ and $V_2 = -\gamma_y V_i^{(0)} - \Delta V_{ret}$. Next consider the probability density function of V_1 . The characteristic function of V_1 , represented as $c_1(\xi)$, is given by

$$\begin{aligned} c_1(\xi) &= c_{RTN}(\xi) \cdot c_n(\xi) \\ &= \frac{1}{i \gamma_y \Delta V_{pp}} \cdot \frac{1}{(1 + \lambda_r^2 \xi^2) \xi} \left[e^{i \gamma_y V_r^{(n)} \xi} - e^{i \gamma_y V_l^{(n)} \xi} \right] \end{aligned} \quad (14)$$

Therefore, the probability density function of V_1 , denoted as $f_1(x)$, can be
 135 calculated as

$$\begin{aligned} f_1(x) &= \frac{1}{2\pi} \int_{-\infty}^{+\infty} e^{-i\xi x} c_1(\xi) d\xi \\ &= \frac{1}{2\gamma_y \Delta V_{pp}} [q(t_1(x)) - q(t_2(x))] \end{aligned} \quad (15)$$

where

$$q(t) = \frac{1}{\pi i} \int_{-\infty}^{+\infty} \frac{1}{(1 + \lambda_r^2 \xi^2) \xi} e^{i\xi t} d\xi \quad (16)$$

and

$$\begin{bmatrix} t_1(x) \\ t_2(x) \end{bmatrix} = \begin{bmatrix} \gamma_y V_r^{(n)} - x \\ \gamma_y V_l^{(n)} - x \end{bmatrix} \quad (17)$$

Define

$$Q(z) = \frac{1}{\lambda_r^2 ((1/\lambda_r^2) + z^2) z} e^{izt} \quad (18)$$

which have three simple poles in the real axis: $z_0 = 0$, $z_1 = i/\lambda_r$ and $z_2 = -i/\lambda_r$.

140 Based on residue theory, we get the result below for the integral in (16):

$$q(t) = \begin{cases} 1 - e^{-\frac{1}{\lambda_r} t} & t \geq 0 \\ -1 + e^{\frac{1}{\lambda_r} t} & t < 0 \end{cases} \quad (19)$$

Next we consider the probability density function of V_2 . The characteristic
 function of V_2 , represented as $c_2(\xi)$, is given by

$$\begin{aligned} c_2(\xi) &= c_e(\xi) \cdot c_{ret}(\xi) \\ &= e^{-\frac{1}{2}(\sigma_c^2 \gamma_y^2 + \sigma_d^2) \xi^2} \cdot e^{i(-\mu_d - \mu_e \gamma_y) \xi} \end{aligned} \quad (20)$$

The probability density function of V_2 , denoted as $f_2(x)$, can be further obtained by

$$\begin{aligned} f_2(x) &= \frac{1}{2\pi} \int_{-\infty}^{+\infty} e^{-i\xi x} c_2(\xi) d\xi \\ &= \frac{1}{\sqrt{2\pi(\sigma_e^2 \gamma_y^2 + \sigma_d^2)}} e^{\frac{-(x+\mu_d+\mu_e \gamma_y)^2}{2(\sigma_e^2 \gamma_y^2 + \sigma_d^2)}} \end{aligned} \quad (21)$$

145 With the results above, $\tilde{p}_{(n)}(x)$ ($1 \leq n \leq K-1$) can be determined by convolving $f_1(x)$ and $f_2(x)$:

$$\begin{aligned} \tilde{p}_{(n)}(x) &= f_1(x) \otimes f_2(x) \\ &= \int_{-\infty}^{+\infty} f_1(\tau) f_2(x-\tau) d\tau \end{aligned} \quad (22)$$

Let $B = -\mu_d - \mu_e \gamma_y$, $C = \sqrt{\sigma_e^2 \gamma_y^2 + \sigma_d^2}$, and define

$$\zeta(x, \omega, v) = \text{erf} \left(\frac{-x + \omega}{\sqrt{2v}} \right) \quad (23)$$

The final expression of $\tilde{p}_{(n)}(x)$ ($1 \leq n \leq K-1$) is given in (24).

$$\begin{aligned} \tilde{p}_{(n)}(x) &= \frac{1}{2\gamma_y \Delta V_{pp}} [q(t_1(x)) \otimes f_2(x) - q(t_2(x)) \otimes f_2(x)] \\ &= \frac{1}{2\gamma_y \Delta V_{pp}} \cdot \left[\zeta(x, B + \gamma_y V_r^{(n)}, C) - \zeta(x, B + \gamma_y V_l^{(n)}, C) \right] + \\ &\quad \frac{e^{\frac{C^2}{2\lambda_r^2}}}{4\gamma_y \Delta V_{pp}} \cdot \left[e^{\frac{1}{\lambda_r}(-x+B+\gamma_y V_r^{(n)})} \left(1 - \zeta(x, B + \gamma_y V_r^{(n)} + \frac{C^2}{\lambda_r}, C) \right) \right. \\ &\quad + e^{-\frac{1}{\lambda_r}(-x+B+\gamma_y V_l^{(n)})} \left(1 + \zeta(x, B + \gamma_y V_l^{(n)} - \frac{C^2}{\lambda_r}, C) \right) \\ &\quad - e^{-\frac{1}{\lambda_r}(-x+B+\gamma_y V_r^{(n)})} \left(1 + \zeta(x, B + \gamma_y V_r^{(n)} - \frac{C^2}{\lambda_r}, C) \right) \\ &\quad \left. - e^{\frac{1}{\lambda_r}(-x+B+\gamma_y V_l^{(n)})} \left(1 - \zeta(x, B + \gamma_y V_l^{(n)} + \frac{C^2}{\lambda_r}, C) \right) \right], \quad (1 \leq n \leq K-1) \end{aligned} \quad (24)$$

For $n = 0$, the probability density function $\tilde{p}_{(n)}(x)$ can be calculated by
 150 convolving $p_r(x)$ and $p_{ret}(x)$ as below:

$$\begin{aligned}\tilde{p}_{(0)}(x) &= \int_{-\infty}^{+\infty} p_r(x + \tau) p_{ret}(\tau) d\tau \\ &= \frac{1}{2\lambda_r} \cdot \frac{1}{\sqrt{2\pi}\sigma_d} \int_{-\infty}^{+\infty} e^{-\frac{|\tau|}{\lambda_r}} \cdot e^{-\frac{(x-\tau+\mu_d)^2}{2\sigma_d^2}} d\tau\end{aligned}\quad (25)$$

The final expression of $\tilde{p}_{(0)}(x)$ is given in (26).

$$\begin{aligned}\tilde{p}_{(0)}(x) &= \frac{1}{4\lambda_r} \cdot e^{\frac{\sigma_d^2}{2\lambda_r^2}} \cdot \left[e^{\frac{1}{\lambda_r}(x+\mu_d)} \left(1 + \zeta(x, -\mu_d - \frac{1}{\lambda_r}\sigma_d^2, \sigma_d) \right) + \right. \\ &\quad \left. e^{-\frac{1}{\lambda_r}(x+\mu_d)} \left(1 - \zeta(x, -\mu_d + \frac{1}{\lambda_r}\sigma_d^2, \sigma_d) \right) \right]\end{aligned}\quad (26)$$

According to (8), the overall distribution of total noises-induced threshold voltage shifts, i.e., $\tilde{p}(x)$ is given in (27).

$$\begin{aligned}\tilde{p}(x) &= \frac{1}{K} \times \sum_{n=0}^{K-1} \tilde{p}_{(n)}(x) \\ &= \frac{1}{2\gamma_y \Delta V_{pp} K} \cdot \sum_{n=1}^{K-1} \left[\zeta(x, B + \gamma_y V_r^{(n)}, C) - \zeta(x, B + \gamma_y V_l^{(n)}, C) \right] + \\ &\quad \frac{e^{\frac{C^2}{2\lambda_r^2}}}{4\gamma_y \Delta V_{pp} K} \cdot \sum_{n=1}^{K-1} \left[e^{\frac{1}{\lambda_r}(-x+B+\gamma_y V_r^{(n)})} \left(1 - \zeta(x, B + \gamma_y V_r^{(n)} + \frac{C^2}{\lambda_r}, C) \right) \right. \\ &\quad + e^{-\frac{1}{\lambda_r}(-x+B+\gamma_y V_l^{(n)})} \left(1 + \zeta(x, B + \gamma_y V_l^{(n)} - \frac{C^2}{\lambda_r}, C) \right) \\ &\quad - e^{-\frac{1}{\lambda_r}(-x+B+\gamma_y V_r^{(n)})} \left(1 + \zeta(x, B + \gamma_y V_r^{(n)} - \frac{C^2}{\lambda_r}, C) \right) \\ &\quad \left. - e^{\frac{1}{\lambda_r}(-x+B+\gamma_y V_l^{(n)})} \left(1 - \zeta(x, B + \gamma_y V_l^{(n)} + \frac{C^2}{\lambda_r}, C) \right) \right] \\ &\quad + \frac{1}{4\lambda_r K} \cdot e^{\frac{\sigma_d^2}{2\lambda_r^2}} \left[e^{\frac{1}{\lambda_r}(x+\mu_d)} \left(1 + \zeta(x, -\mu_d - \frac{1}{\lambda_r}\sigma_d^2, \sigma_d) \right) \right. \\ &\quad \left. + e^{-\frac{1}{\lambda_r}(x+\mu_d)} \left(1 - \zeta(x, -\mu_d + \frac{1}{\lambda_r}\sigma_d^2, \sigma_d) \right) \right]\end{aligned}\quad (27)$$

Since channel parameters (specifically B , C , σ_d , and μ_d) vary for different
155 levels in the flash channel, the overall noise density functions in respect to
all K levels (denoted as $L_0 \rightarrow L_{K-1}$) are not exactly the same. Denote the
probability density functions of noise-induced threshold voltage shifts for $L_0 \rightarrow$
 L_{K-1} as $\tilde{p}^{(k)}(x)$, ($0 \leq k \leq K-1$). Based on 2 bits/cell NAND flash memory and
the parameters presented in the literature [8], we simulated the distributions
160 of noise-induced threshold voltage shifts and compared the results with the
theoretical counterparts found in (27).

Simulations: The normalized σ_e and μ_e of the erased state are set as 0.35
and 1.4, respectively. For the three programmed states, we set the normalized
program step voltage ΔV_{pp} as 0.2, and the normalized verify voltages V_p as
165 2.6, 3.2, and 3.93, respectively. For the RTN distribution function $p_r(x)$, we
set the parameter $\lambda_r = K_\lambda \cdot N^{0.5}$, where K_λ equals to 0.00025. Regarding
CCI, we ignore the CCI from the two diagonal directions and also fix γ_y to a
constant 0.08. For the function $\mathcal{N}(\mu_d, \sigma_d^2)$ to capture trap recovery and electron
detrapping during retention, we assume that μ_d scales with $N^{0.5}$ and σ_d^2 scales
170 with $N^{0.6}$, and both scale with $\ln(1+t/t_0)$, where t denotes the memory retention
time and t_0 is an initial time set as 1 hour. In addition, both μ_d and σ_d^2 also
depend on the initial threshold voltage. Hence we set that both approximately
scale $K_s(x - x_0)$, where x is the initial threshold voltage, and x_0 and K_s are
constants. Therefore, we have

$$\begin{cases} \mu_d = K_s(x - x_0)K_d N^{0.5} \ln(1 + \frac{t}{t_0}) \\ \sigma_d^2 = K_s(x - x_0)K_m N^{0.6} \ln(1 + \frac{t}{t_0}) \end{cases} \quad (28)$$

175 where we set $K_s = 0.38$, $x_0 = 1.4$, $K_d = 4 \times 10^{-4}$ and $K_m = 4 \times 10^{-6}$ [8].

Setting the P/E cycling number N as 1000, and the retention time as 1 year,
we found the probability density based on (27) for channel noises occurring in
all four levels, respectively, as illustrated in Fig. 2.

Accordingly, we carry out Monte Carlo simulations to obtain the cell thresh-
180 old voltage distribution at different levels under 1000 P/E cycling and 1 year
retention limit, as shown in Fig. 3, which gives nearly the same results as in

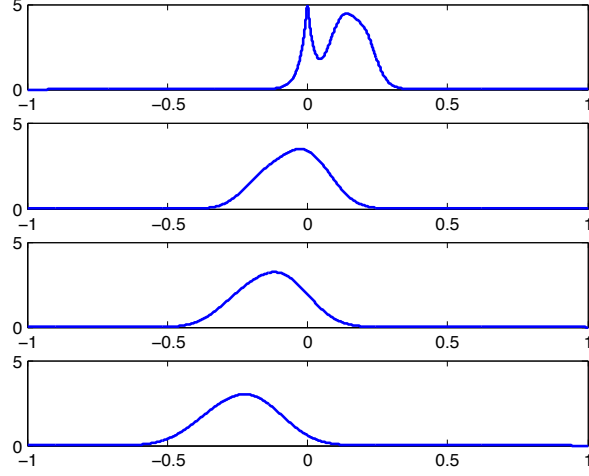


Figure 2: Theoretical curves to show the effects of RTN, CCI, and retention noises on memory cell threshold voltage distribution after 1K P/E cycling and 1 year retention.

Fig. 2. A close resemblance supports the correctness of the above theoretical derivations on the noises-induced threshold voltage shifts.

3.2. Cell Threshold Voltage Distribution

185 In this section, the threshold voltage distribution of each level is determined, which can be used to calculate the log-likelihood ratio (LLR) of each bit stored in the memory, and further used for flash coding [11].

As shown in Fig. 2, the curves for $L_1 \rightarrow L_3$ are bell-shaped, which is due to the fact that retention noise becomes dominant as the P/E cycling number and
 190 the retention time increase. Therefore, we intuitively expect a Gaussian distribution will be a good fit for these probability density functions. The formulas below give the curve-fitting parameters of the proposed normal distribution ($1 \leq k \leq K - 1$).

$$\mu_{(k)} = \int_{-\infty}^{+\infty} x \cdot \tilde{p}^{(k)}(x) dx. \quad (29)$$

$$\sigma_{(k)}^2 = \int_{-\infty}^{+\infty} (x - \mu_{(k)})^2 \cdot \tilde{p}^{(k)}(x) dx. \quad (30)$$

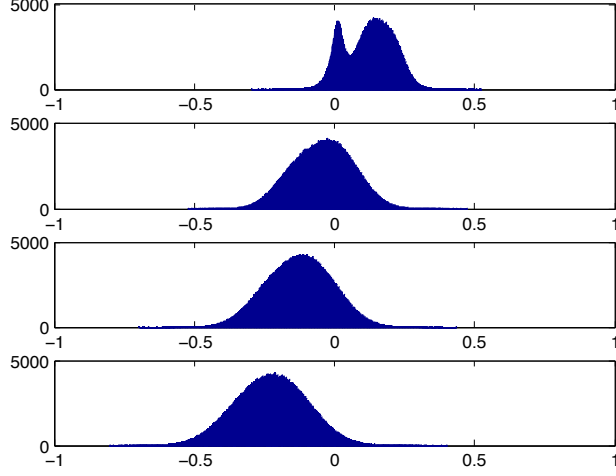


Figure 3: Simulated curves to show the effects of RTN, CCI, and retention noises on memory cell threshold voltage distribution after 1K P/E cycling and 1 year retention.

$$\begin{aligned}
p^{(k)}(x) &= g^{(k)}(x) \otimes p_i^{(k)}(x) = g^{(k)}(x) \otimes p_p^{(k)}(x) = \int_{-\infty}^{+\infty} p_p^{(k)}(\tau) g^{(k)}(x - \tau) d\tau \\
&= \int_{V_l^{(k)}}^{V_r^{(k)}} \frac{1}{\Delta V_{pp}} \cdot \frac{1}{\sqrt{2\pi}\sigma_{(k)}} e^{-\frac{(x-\tau-\mu_{(k)})^2}{2\sigma_{(k)}^2}} d\tau \\
&= \frac{1}{2\Delta V_{pp}} \left[\zeta(x, V_r^{(k)} + \mu_{(k)}, \sigma_{(k)}) - \zeta(x, V_l^{(k)} + \mu_{(k)}, \sigma_{(k)}) \right], 1 \leq k \leq K - 1
\end{aligned} \tag{32}$$

Therefore, the probability density function of the curve-fitted normal distributions for $L_1 \rightarrow L_{K-1}$ are given by

$$g^{(k)}(x) = \frac{1}{\sqrt{2\pi}\sigma_{(k)}} e^{-\frac{(x-\mu_{(k)})^2}{2\sigma_{(k)}^2}}, 1 \leq k \leq K - 1. \tag{31}$$

Recall the initial distributions of $L_1 \rightarrow L_{K-1}$ after ideal programming in Eq. (3), we can obtain the final probability density functions, denoted as $p^{(k)}(x)$, by convoluting $g^{(k)}(x)$ and $p_i^{(k)}(x)$. The results are given in (32).

Since the retention noise has minor influence on the threshold voltage of L_0 , the probability density function of L_0 shown in Fig. 2 is not bell-shaped, thus it

would not be correct to use a normal distribution for curve fitting in this case. However, the final distribution of L_0 can be easily determined with the results in (27) as the distribution of L_0 after ideal programming is Gaussian. To this end, the two parameters: μ_d and σ_d in (27), should be revised as follows.

$$\begin{cases} \mu'_d = \mu_d - \mu_e \\ \sigma'_d = \sqrt{\sigma_e^2 + \sigma_d^2} \end{cases} \quad (33)$$

205 Accordingly, B and C , should be revised as well as follows.

$$\begin{cases} B' = -\mu'_d - \mu_e \gamma_y = -\mu_d - \mu_e \gamma_y + \mu_e \\ C' = \sqrt{\sigma_e^2 \gamma_y^2 + \sigma_d'^2} = \sqrt{\sigma_e^2 \gamma_y^2 + \sigma_d^2 + \sigma_e^2} \end{cases} \quad (34)$$

Consequently, the final threshold voltage distribution of L_0 , i.e. $p^{(0)}(x)$, can be calculated in (35).

$$\begin{aligned} p^{(0)}(x) &= \tilde{p}^{(0)}(x) \otimes p_e(x) \\ &= \frac{1}{2\gamma_y \Delta V_{pp} K} \cdot \sum_{n=1}^{K-1} \left[\zeta(x, B' + \gamma_y V_r^{(n)}, C') - \zeta(x, B' + \gamma_y V_l^{(n)}, C') \right] + \\ &\quad \frac{e^{\frac{C'^2}{2\lambda_r^2}}}{4\gamma_y \Delta V_{pp} K} \cdot \sum_{n=1}^{K-1} \left[e^{\frac{1}{\lambda_r}(-x+B'+\gamma_y V_r^{(n)})} \left(1 - \zeta(x, B' + \gamma_y V_r^{(n)} + \frac{C'^2}{\lambda_r}, C') \right) \right. \\ &\quad + e^{-\frac{1}{\lambda_r}(-x+B'+\gamma_y V_l^{(n)})} \left(1 + \zeta(x, B' + \gamma_y V_l^{(n)} - \frac{C'^2}{\lambda_r}, C') \right) \\ &\quad - e^{-\frac{1}{\lambda_r}(-x+B'+\gamma_y V_r^{(n)})} \left(1 + \zeta(x, B' + \gamma_y V_r^{(n)} - \frac{C'^2}{\lambda_r}, C') \right) \\ &\quad \left. - e^{\frac{1}{\lambda_r}(-x+B'+\gamma_y V_l^{(n)})} \left(1 - \zeta(x, B' + \gamma_y V_l^{(n)} + \frac{C'^2}{\lambda_r}, C') \right) \right] \\ &\quad + \frac{1}{4\lambda_r K} \cdot e^{\frac{\sigma_d'^2}{2\lambda_r^2}} \left[e^{\frac{1}{\lambda_r}(x+\mu'_d)} \left(1 + \zeta(x, -\mu'_d - \frac{1}{\lambda_r} \sigma_d'^2, \sigma'_d) \right) \right. \\ &\quad \left. + e^{-\frac{1}{\lambda_r}(x+\mu'_d)} \left(1 - \zeta(x, -\mu'_d + \frac{1}{\lambda_r} \sigma_d'^2, \sigma'_d) \right) \right] \end{aligned} \quad (35)$$

The aforementioned 4-level MLC flash and the related channel parameters have been used as well in this section to show the probability density functions

210 derived above. The P/E cycling number is set as 1000 and retention time as 1
 year. Fig. 4 illustrates the final threshold voltage distributions of all four levels
 according to (32) and (34). As shown, the channel modeled in this work is quite
 similar to the models used in the literatures [5, 4, 7, 8]. Nonetheless, as only
 reasonable Gaussian approximation is used and all the channel noises have been
 215 considered in the derivations above, the model proposed here is more precise
 to the real flash channel. Moreover, the exact formula of cell threshold voltage
 distribution, i.e., the results given in (34), makes the soft decisions calculated
 based on our work more accurate for the flash decoding.

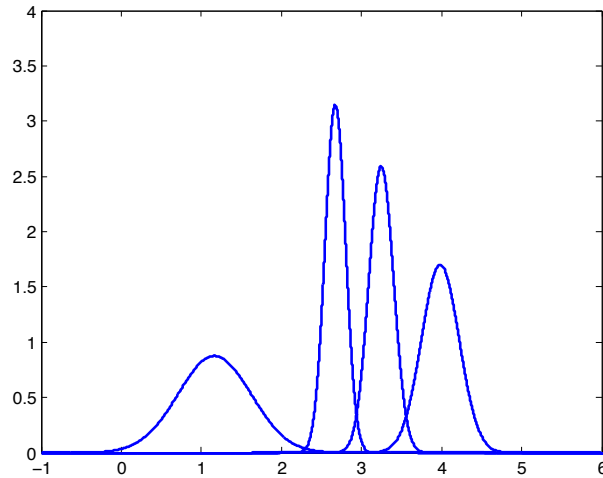


Figure 4: Cell threshold voltage distributions 4-level MLC flash memory

3.3. Calculation of Soft Decisions

220 Soft decisions, or in other words, the log-likelihood-ratios (LLRs) information
 are critical in decoding the advanced flash error correction codes. This section
 proposes the mathematical formulation for calculating LLRs based upon the
 threshold-voltage distributions presented above, and the results are used to
 instruct the implementation of decoding schemes in the design practice.

225 Assume each bit is programmed to a flash cell with equal probability, i.e.,
 all the storage levels in one memory cell have equal *a priori* probability, and let

V_{th} represents the sensed threshold voltage of one memory cell, we can calculate the LLR of the i th bit stored in one cell as

$$L(b_i) = \log \frac{p(b_i = 1|V_{th})}{p(b_i = 0|V_{th})} = \log \frac{p(V_{th}|b_i = 1)}{p(V_{th}|b_i = 0)} \quad (36)$$

For K levels MLC flash memory, there are $N_b = \log_2(K)$ bits stored in each cell, and the probability density function of the threshold voltage of k th storage level, $p^{(k)}(x), 0 \leq k \leq K - 1$, is known from (32) and (35). Let \mathbb{S}_i denote the set of levels whose i th bit is 1. Hence, given the threshold voltage V_{th} of a cell, the LLR of each bit would be calculated as

$$L(b_i) = \log \frac{\sum_{k \in \mathbb{S}_i} p^{(k)}(V_{th})}{\sum_k p^{(k)}(V_{th}) - \sum_{k \in \mathbb{S}_i} p^{(k)}(V_{th})} \quad (37)$$

In respect to practical NAND flash memories, the cell threshold voltages cannot be precisely obtained while being sensed by the comparison with a series of reference voltages. Assume that the threshold voltage V_{th} falls into the range $(R_l, R_r]$ (where R_l and R_r are two adjacent reference voltages), we can estimate the corresponding LLR of the i th bit as

$$L(b_i) = \log \frac{\int_{R_l}^{R_r} \sum_{k \in \mathbb{S}_i} p^{(k)} V_{th}}{\int_{R_l}^{R_r} \sum_k p^{(k)} V_{th} - \int_{R_l}^{R_r} \sum_{k \in \mathbb{S}_i} p^{(k)} V_{th}} \quad (38)$$

We assume the parameters $\sigma_e, \mu_e, \sigma_d, \mu_d$ in (32) and (35) are known and treat the coupling ratio γ_y as a known constant. As the number of reference voltages in memory sensing is fixed, all possible LLRs can be calculated before the decoding starts. Therefore, only a lookup table is required in the run time to obtain the LLRs, which reduces the system complexity and improves the speed and throughput. Let K_s denote the number of reference voltages being used in memory sensing, the LLR lookup table only contains $N_b(K_s + 1)$ entries for N_b -bit/cell NAND flash memory [12].

4. Conclusions

We have derived the probability density function for the channel noises in the MLC NAND flash memories, and formulated the threshold voltage distribution of each symbol. This was possible by using characteristic functions for the various noises. The results presented here are novel in a theoretical way as the first time the flash channel has been characterized by incorporating the distributions of all the interferences and noises. Using the 4-level MLC flash as a case study, the derived threshold voltage distributions were demonstrated to be consistent with simulated channel outputs.

References

- [1] R. Gallager, Low-density parity check codes, *IRE Trans. Information Theory* (1962) 21–28.
- [2] X. Hu, B. Kumar, Z. Li, R. Barndt, Error Floor Estimation of Long LDPC Codes on Partial Response Channels, in: *IEEE GLOBECOM*, 2007, pp. 259–264.
- [3] Q. Xu, T. Chen, Y. Hu, P. Gong, Write Pattern Format Algorithm for Reliable NAND-Based SSDs, *IEEE Trans. on Circuits and Systems II: Express Briefs* 61 (7) (2014) 516–520.
- [4] J. Wang, T. Courtade, H. Shankar, R. Wesel, Soft information for LDPC decoding in flash: mutual-information optimized quantization, in: *IEEE GLOBECOM*, 2011, pp. 1–6.
- [5] F. Sun, S. Devarajan, K. Rose, T. Zhang, Multilevel flash memory on-chip error correction based on trellis coded modulation, in: *2006 IEEE Int. Symp. on Circuits and Systems (ISCAS 2006)*, 2006.
- [6] H. Zhou, A. Jiang, J. Bruck, Error-correcting schemes with dynamic thresholds in non-volatile memories, in: *International Symposium on Information Theory*, 2011, pp. 2143–2147.

- [7] D. hwan Lee, W. Sung, Estimation of NAND Flash Memory Threshold
275 Voltage Distribution for Optimum Soft-Decision Error Correction, *IEEE
Trans. on Signal Processing* 61 (2) (2013) 440–449.
- [8] G. Dong, Y. Pan, N. Xie, C. Varanasi, T. Zhang, Estimating Information-
Theoretical NAND Flash Memory Storage Capacity and its Implication to
Memory System Design Space Exploration, *IEEE Trans. on Very Large
280 Scale Integration (VLSI) Systems* 20 (9) (2012) 1705–1714.
- [9] J. Moon, J. No, S. Lee, S. Kim, S. Choi, Y. Song, Statistical Characteri-
zation of Noise and Interference in NAND Flash Memory, *IEEE Trans. on
Circuits and Systems I: Regular Papers* 60 (8) (2013) 2153–2164.
- [10] J. Moon, J. No, S. Lee, S. Kim, J. Yang, Statistical Analysis of Flash
285 Memory Read Data, in: *IEEE GLOBECOM*, 2011, pp. 1–6.
- [11] G. Dong, S. Li, T. Zhang, Using Data Postcompensation and Predistortion
to Tolerate Cell-to-cell Interference in MLC NAND Flash Memory, *IEEE
Trans. on Circuit and System: Part I* (2010) 2718–2728.
- [12] G. Dong, N. Xie, T. Zhang, On the use of soft-decision error-correction
290 codes in nand flash memory, *IEEE Trans. on Circuits and Systems I: Reg-
ular Papers* 58 (2) (2011) 429–439.